SCIENCE CHINA
Information Sciences

• RESEARCH PAPER •

June 2023, Vol. 66 162302:1–162302:16
https://doi.org/10.1007/s11432-022-3595-y

MIMO performance enhancement of MIMO arrays using PCS-based near-field optimization technique

Yipeng WANG[1], Xiaoming CHEN[1*], Huiling PEI[1], Wei E. I. SHA[2], Yi HUANG[3] & Ahmed A. KISHK[4]

[1]*School of Information and Communications Engineering, Xi'an Jiaotong University, Xi'an* 710049*, China;*
[2]*Key Laboratory of Micro-Nano Electronic Devices and Smart Systems of Zhejiang Province, College of Information Science and Electronic Engineering, Zhejiang University, Hangzhou* 310027*, China;*
[3]*Department of Electrical Engineering and Electronics, University of Liverpool, Liverpool* L69 3GJ*, UK;*
[4]*Department of Electrical and Computer Engineering, Concordia University, Montreal* QC 3F 1M8*, Canada*

Received 14 June 2022/Revised 22 August 2022/Accepted 4 October 2022/Published online 10 May 2023

Abstract Extensive efforts have been made in designing large multiple-input multiple-output (MIMO) arrays. Nevertheless, improvements in conventional antenna characteristics cannot ensure significant MIMO performance improvement in realistic multipath environments. Array decorrelation techniques have been proposed, achieving correlation reductions by either tilting the antenna beams or shifting the phase centers away from each other. Hence, these methods are mainly limited to MIMO terminals with small arrays. To avoid such problems, this work proposes a decorrelation optimization technique based on phase correcting surface (PCS) that can be applied to large MIMO arrays, enhancing their MIMO performances in a realistic (non-isotropic) multipath environment. First, by using a near-field channel model and an optimization algorithm, a near-field phase distribution improving the MIMO capacity is obtained. Then the PCS (consisting of square elements) is used to cover the array's aperture, achieving the desired near-field phase distribution. Two examples demonstrate the effectiveness of this PCS-based near-field optimization technique. One is a 1×4 dual-polarized patch array (working at 2.4 GHz) covered by a 2×4 PCS with 0.6λ center-to-center distance. The other is a 2×8 dual-polarized dipole array, for which a 4×8 PCS with 0.4λ center-to-center distance is designed. Their MIMO capacities can be effectively enhanced by 8% and 10% in single-cell and multi-cell scenarios, respectively. The PCS has insignificant effects on mutual coupling, matching, and the average radiation efficiency of the patch array, and increases the antenna gain by about 2.5 dB while keeping broadside radiations to ensure good cellular coverage, which benefits the MIMO performance of the array. The proposed technique offers a new perspective for improving large MIMO arrays in realistic multipath in a statistical sense.

Keywords antenna correlation, array antenna, multiple-input multiple-output (MIMO) capacity

Citation Wang Y P, Chen X M, Pei H L, et al. MIMO performance enhancement of MIMO arrays using PCS-based near-field optimization technique. Sci China Inf Sci, 2023, 66(6): 162302, https://doi.org/10.1007/s11432-022-3595-y

1 Introduction

Multiple-input multiple-output (MIMO) techniques have been adopted ubiquitously in the fourth generation (4G) and fifth generation (5G) cellular systems thanks to the enhanced spectral efficiency [1–3]. Due to the space limitation and the limited angular spread of the propagation channel [1], correlations inevitably occur between the MIMO array elements, which can significantly degrade the MIMO performance [1, 2, 4]. Many studies tried to reduce the correlation by minimizing the mutual coupling in the MIMO antenna using different methods, assuming (implicitly) that the incoming waves are uniformly distributed in the three-dimensional (3D) multipath environment, such as metamaterials or metasurface [5–7], stacked patch design [8], combining a monopole and a pair of inverted-L antennas (ILAs) with 180° out-of-phase excitations [9], slitted ground plane [10], ground branch [11], suspended microstrip

* Corresponding author (email: xiaoming.chen@mail.xjtu.edu.cn)

line [12], electromagnetic band gap (EBG) [13, 14], and differential modes cancellation [15]. However, it has been shown that, in a realistic non-uniform multipath environment, reducing mutual coupling does not guarantee reduced correlation [16]. Ref. [17] proposed a pixelated ground surface to enhance the MIMO capacity. The mutual coupling was greatly suppressed, while correlation information was not given. The correlation is more complex than the mutual coupling between antenna elements and it depends not only on the MIMO antenna radiation patterns but also on the propagation channel [16, 18]. Although the propagation channel is inherent in the multipath environment that cannot be changed, it is certainly possible to reduce the correlation (and, therefore, enhance the MIMO capacity) by making the radiation patterns orthogonal to each other [19–25]. Ref. [19] tilted the main beams of two patch antennas away from each other by placing a frequency selective surface (FSS) above a 1×2 patch array, which reduces the correlation at the expense of increased mutual coupling. The same idea has been extended to 6-port (2×3) and 4-port dielectric resonator antenna (DRA) arrays with enhanced isolations in [20, 26], respectively. Moreover, the array isolations have been improved as well in these studies. Nevertheless, these studies assumed a 3D uniform scattering environment, and the proposed beam-tilting method is challenging to be extended to large arrays. In [21], optimal radiation patterns were calculated by considering the power angular spectrum (PAS) of the multipath environment. Nevertheless, the work was limited to 2D propagation scenarios. Moreover, it only results in optimal source current distribution without considering how to excite it in actual antennas. Ref. [22] improved the channel eigenspace of a massive MIMO system by placing wire grid FSSs in the vicinity of the base station (BS) array. But they assumed a pure line-of-sight scenario and had only a simulation demonstration. It is unclear how to extend the scheme to the multipath scenario. It is shown in [24] that by placing a scatterer array with identical elements in front of the array antenna, the equivalent phase centers of the array elements can be stretched, leading to larger equivalent inter-element spacing and, therefore, lower correlations. By placing several identical scatterer elements at different heights over the array to modify the near-field phase distribution to resemble an array with larger inter-element separation [25], the MIMO performance can be enhanced (although the design approach is different, it also increases the distances between phase centers). Recently, it is shown that a similar decorrelation scheme can be used in combination with certain decoupling techniques to improve correlation and isolation at the same time [27]. Nevertheless, both schemes become less effective for linear arrays with more than four elements. It should be noted that the complex-valued radiation patterns and the angular distribution together determine the correlations between the array elements. Hence, it is insufficient to judge the orthogonality of the radiation patterns by looking at the amplitude patterns alone. In other words, one can design orthogonal array patterns by exploiting the phase patterns without tilting the antenna beams. As mentioned before, decorrelation and decoupling can be achieved simultaneously for compact MIMO arrays [20, 23, 26, 27]. For MIMO arrays with half-wavelength inter-element spacing, the mutual coupling can be sufficiently low already. Thus, decoupling is not needed. If an isotropic scattering environment is assumed, the antenna correlations will be negligible. Nevertheless, in a realistic multipath environment with limited angular spread, the correlation between two half-wavelength separated antenna elements can still be high [1, 18, 24, 25, 27], and array decorrelation is necessary in order to improve the MIMO performance.

In this paper, we propose a phase correcting surface (PCS)-based near-field optimization technique to reduce the antenna correlation and increase the MIMO capacity of the array antenna in multipath environments with various angular spreads. Unlike the previous methods of increasing the equivalent distances between array elements [24, 25], the array's better MIMO performance can be achieved by optimizing the phase distribution of the planar near-field channel at a distance above the array to improve the orthogonality of the array's radiation patterns. Then this better phase distribution is approximately achieved by discretized phase correcting elements. It is shown that by using this technique, the correlations are reduced, and the MIMO capacity is enhanced effectively. Unlike the beam tilting-based decorrelation methods [19, 20, 26], the proposed PCS achieves array decorrelation by modifying the array's near-field phase distribution while keeping broadside radiations. This feature is essential to ensure good cellular coverage for BS applications. Therefore, as opposed to the previous studies, the proposed technique is applicable for large arrays at the BS or access point (AP) in multipath environments, which is vital for massive MIMO communications.

2 MIMO performance metrics

For the sake of completeness, we briefly introduce some relevant MIMO performance metrics here.

2.1 MIMO capacity

The ultimate goal of the MIMO array design is to enhance the MIMO capacity. The MIMO capacity C can be expressed as [1]

$$C = \log_2 \det\Big[\boldsymbol{I} + \frac{\gamma}{N}\boldsymbol{H}\boldsymbol{H}^{\mathrm{H}}\Big], \tag{1}$$

where $\boldsymbol{H}$ is the MIMO channel matrix, $\boldsymbol{I}$ denotes an identity matrix, γ is the reference signal-to-noise-ratio (SNR), N is the number of transmitting antennas, $\log_2$ signifies the logarithm operator of base 2, det denotes the determinant operator, and the superscript H is the Hermitian (conjugate transpose) operator. The MIMO channel matrix $\boldsymbol{H}$ is obtained from the radiation patterns of the array elements and incident waves of the MIMO channel. Specifically, the radiation patterns of the MIMO antennas are imported to a ray-tracing channel model described in [16]. The channel coefficients are emulated by impinging incident waves on the radiation patterns [16, 21].

The MIMO capacity expression itself offers limited guidance on the optimal design of MIMO antennas. To show the correlations' effect, we resort to the well-known Kronecker channel model

$$\boldsymbol{H} = \boldsymbol{R}_r^{1/2}\boldsymbol{H}_w\boldsymbol{R}_t^{1/2}, \tag{2}$$

where $\boldsymbol{H}_w$ denotes the spatially white (uncorrelated) MIMO channel, the superscript $1/2$ is the Hermitian square root operator, $\boldsymbol{R}_t$ and $\boldsymbol{R}_r$ are correlation matrices of the transmitting and receiving arrays, respectively. For notational convenience, we will drop the subscripts of $\boldsymbol{R}_t$ and $\boldsymbol{R}_r$ hereafter when it is clear from the context or when it is less important to distinguish the correlations at either end of a MIMO system.

2.2 Antenna correlations and diversity

It is clear from Subsection 2.1 that the correlation matrices play an important role in the MIMO capacity. It is well known that high correlations between the array antenna elements tend to degrade the MIMO capacity [1]. Moreover, unlike the capacity, the correlation coefficients (i.e., the entries of the correlation matrix) can be explicitly expressed using the antenna characteristics.

For a MIMO array at the receiving side, the correlation coefficient between array elements n and m can be expressed in terms of their (complex-valued embedded) radiation patterns as [18]

$$\begin{aligned} r_{mn} &= \frac{\oint |G_{12}(\Omega)|\mathrm{d}\Omega}{\sqrt{\oint |G_{11}(\Omega)|\mathrm{d}\Omega}\sqrt{\oint |G_{22}(\Omega)|\mathrm{d}\Omega}}, \\ G_{mn}(\Omega) &= \kappa E_{\theta m}(\Omega)E^*_{\theta n}(\Omega)P_\theta(\Omega) + E_{\phi m}(\Omega)E^*_{\phi n}(\Omega)P_\phi(\Omega), \end{aligned} \tag{3}$$

where κ represents the cross-polarization discrimination (XPD) of the propagation channel, the superscript $*$ denotes the complex conjugate operator, $E_{\theta n}$ and $E_{\phi n}$ are the θ and ϕ polarized components of the radiation pattern of the nth array element, $P_\theta(\Omega)$ and $P_\phi(\Omega)$ are the PAS of θ and ϕ polarized incoming waves from the solid angle Ω, respectively, and they are linked to the propagation channel. Likewise, the correlation coefficients at the receiving array can be determined. It is clear from the correlation expression (3) that the correlation coefficients depend on the radiation patterns and the propagation channel. While the latter is inherent in the multipath environment that we cannot change, it is possible to reduce the correlation (and, therefore, enhance the MIMO capacity) by optimizing the MIMO antenna, which is the ultimate goal of this work.

The correlation expressions (3) are mainly helpful for theoretical analysis. To calculate the correlation coefficients from simulated or measured multipath channels [28], the following equation is usually used:

$$r_{mn} = \frac{\boldsymbol{E}\left[s_m s_n^*\right]}{\sqrt{\boldsymbol{E}\left[|s_m|^2\right]\boldsymbol{E}\left[|s_n|^2\right]}}, \tag{4}$$

where s_m is the received signal at the mth array element in the multipath environment and $\boldsymbol{E}$ denotes the mathematical expectation operator. As long as the incoming wave angular distribution is accurately described by $P_\theta(\Omega)$ and $P_\phi(\Omega)$ with known XPD, Eqs. (3) and (4) essentially yield the same result.

The correlation coefficient is a commonly used performance metric for MIMO antennas, and it can be conveniently used to characterize the correlation performance of arrays with only a few antenna

ports. However, the number of correlation coefficients increases rapidly as the number of array elements grows, making it cumbersome to characterize the correlation performance. Moreover, multiple correlation coefficients make it challenging to compare the arrays' correlation performances. For instance, r_{12} of Array 1 is larger than that of Array 2, whereas r_{23} of Array 1 is smaller than that of Array 2, in which case, it is difficult to tell which array has a better correlation performance.

In order to compare the correlation performances conveniently and unambiguously, one can resort to the diversity measure [29] or the degree of freedom (DoF) [30],

$$\mathrm{DoF} = \frac{\mathrm{tr}(\boldsymbol{R})^2}{\mathrm{tr}\,(\boldsymbol{R}^2)}, \tag{5}$$

where $\mathrm{tr}(\boldsymbol{R})$ denotes the trace of the correlation matrix $\boldsymbol{R}$. The diversity measure indicates the equivalent number of uncorrelated elements of an array, which ranges from the minimum value of 1 (i.e., fully correlated array) to the maximum value of N (i.e., the number of array elements for totally uncorrelated array). Using the DoF, one can evaluate the correlation performance of an array using a single scalar instead of multiple correlation coefficients. More importantly, one can readily compare the correlation performances of different arrays without ambiguity. Therefore, the diversity measure is adopted for correlation performance evaluation in this work.

3 Decorrelation optimization technique

From an algorithmic perspective, making the radiation patterns in the horizontal plane mutually orthogonal, leading to the lowest correlation of the arrays, is a brilliant way of optimizing existing arrays for greater MIMO performance [21]. The pattern synthesis method [31] can achieve desired radiation patterns for newly designed arrays. However, in practical applications, introducing decorrelation structures near arrays is a helpful method to affect the existing arrays' radiation patterns [19, 22]. We propose a decorrelation optimization technique based on these observations. This technology can theoretically obtain a near-field phase distribution that lowers array correlation through the near-field channel model. Then it uses the PCS to achieve the better phase distribution. This section presents the near-field channel model and the optimization method.

3.1 Near-field channel model

We first model the near-field channel using spherical waves, since the region of interest is close to the antennas [32, 33]. The near-field channel model describes the spherical wave phase relationship between the planar near-field sampling points above the array and the positions of the antenna elements. There are m subchannels between each antenna element and the sampling points at the sampling plane above the array, as shown in Figure 1. We model the channel using the planar near-field partly because it can more conveniently characterize the effect of the planar PCS structure on the channel. On the other hand, the far-field radiation pattern of the array, which is required for evaluating MIMO capacity and diversity, can also be easily calculated using the planar near- to far-field transformation algorithm. For convenience, we only assume a MIMO array with N single-polarized antenna elements (the case of dual-polarized arrays can be easily extended). In the near-field channel model, when the i antenna element is excited, the electric field on the two-dimensional sampling plane above the array will be defined in matrix form as $\boldsymbol{B}_{i_{\mathrm{wo}}}$, as shown in Figure 1(a). After loading the PCS with q elements between the array and the sampling plane (see Figure 1(b)), for the subchannel p, the new E-field (an entry of $\boldsymbol{B}_{i_{\mathrm{wi}}}$) on the plane can be expressed as

$$\boldsymbol{E}_{ip_{\mathrm{wi}}} = \boldsymbol{E}_{ip_{\mathrm{wo}}} \cdot \mathrm{e}^{\mathrm{j}\phi_s}, \tag{6}$$

where ϕ_s is the phase shift introduced by PCS in subchannel p. It is worth noting that this channel model has two prior assumptions, both of which are intended to reduce the complexity of the model. First of all, the PCS needs to maintain a high transmission coefficient to reduce the blocking of the array radiation. Therefore we ignore the path loss introduced by it. Secondly, for convenience, the phase shift introduced by PCS in each subchannel mainly refers to the phase shift of each PCS element in the normal direction. The definition of the phase shift and the setup in the CST Studio Suite is shown in Figure 2. A parametric study of the unit-cell element is usually performed to obtain the required transmission characteristics of the PCS elements. The PCS element is simulated in a unit-cell, as shown in Figure 2, with periodic

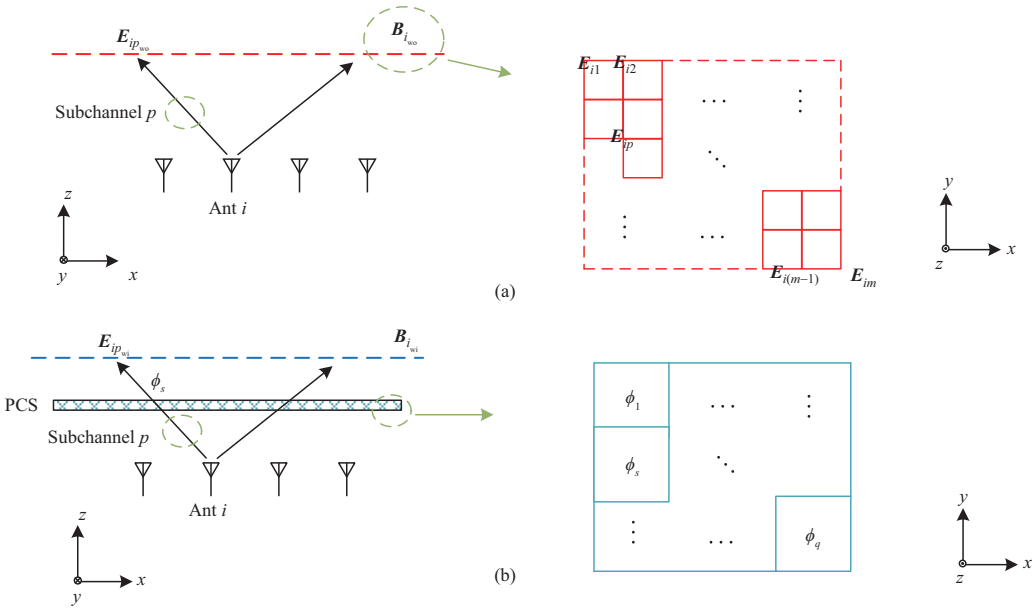

Figure 1 (Color online) Near-field channel model of the array (a) without and (b) with PCS.

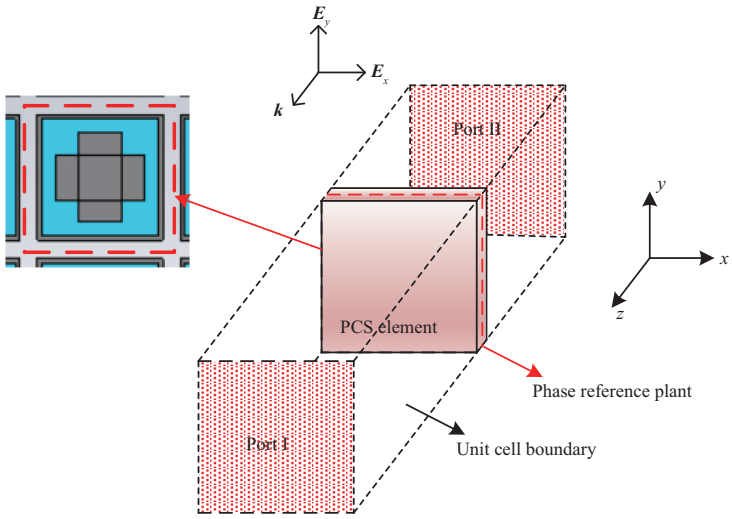

Figure 2 (Color online) Simulation setup in the CST Studio Suite.

boundary conditions [34], which mimics the periodic environment of the elements. In the simulation, the PCS element is illuminated by a transverse electromagnetic wave (TEM) wave traveling along the z-axis. The S-parameter phase between two ports is the phase shift needed if the phase reference plane is set in the middle of the PCS element, as shown in Figure 2.

3.2 Orthogonal basis matrix

Array's radiation patterns required to determine MIMO capacity and diversity can be estimated from the planar near-field using the near- to far-field transformation algorithm method [35]. However, during the optimization process, this transformation approach is time- and resource-consuming to repeatedly determine the array's radiation patterns as the phase shift distribution of PCS changes. Therefore, a fast and simplified method should be applied in the optimization process. This subsection proposes an orthogonal basis matrix-based near- to far-field transformation algorithm that only needs to be applied once before optimizing existing MIMO arrays.

Assume that a y-polarized antenna is placed at the origin of the Cartesian coordinate system and radiates in the positive direction of the z axis, as shown in Figure 3. The far-field radiation pattern of

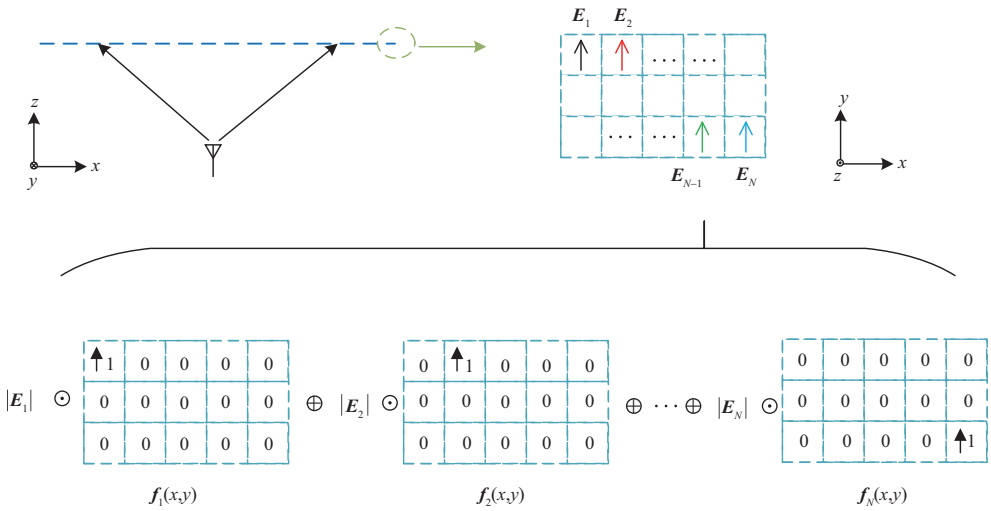

Figure 3 (Color online) Orthogonal basis representation of planar near field.

the antenna can be calculated using the fixed phase method as [35]

$$\begin{aligned}
&\boldsymbol{E}(\theta,\phi) = \mathrm{j}\frac{\mathrm{e}^{-\mathrm{j}kr}}{\lambda r}\cos\theta \boldsymbol{F}(k_x,k_y),\\
&k_x = k_0\sin\theta\cos\phi,\\
&k_y = k_0\sin\theta\sin\phi,\\
&k_z = k_0\cos\theta,
\end{aligned} \tag{7}$$

where r is the distance from the observation point to the origin, λ is the wavelength of free space, (θ, ϕ) is the azimuth, k_x and k_y are the wavenumber components in the x and y directions, respectively. $\boldsymbol{F}(k_x,k_y)$ is the plane wave spectrum [35], which can be expressed as

$$\boldsymbol{F}(k_x,k_y) = \iint \boldsymbol{E}_T(x,y,z=l)\mathrm{e}^{\mathrm{j}(k_x x+k_y y)}\mathrm{d}x\mathrm{d}y, \tag{8}$$

where $\boldsymbol{E}_T(x,y,z=l)$ represents the tangential E-field on the sampling plane at $z=l$, which can be expressed as a weighted sum of a set of N orthogonal bases $\boldsymbol{f}_n(x,y)$:

$$\boldsymbol{E}_T(x,y) = \sum_n B_n \boldsymbol{f}_n(x,y), \tag{9}$$

where $n=1,\ldots,N$. When the plane orthogonal basis $\boldsymbol{f}_n(x,y)$ illustrated in Figure 3 is employed, the E-field on the sampling plane can be represented as the sum of the products of the E-field $\boldsymbol{E}_n$ (B_n shown in (9)) at each sampling point and the associated plane orthogonal basis $\boldsymbol{f}_n(x,y)$. In the simulation, E-field at each sampling point (B_n) can be obtained by setting E-field monitors in the CST Studio Suite, while for a real BS array, a planar nearfield scanner (PNFS) [35] in an anechoic chamber can be used. Combining Eqs. (7)–(9), the far-field radiation pattern can be expressed as

$$\begin{aligned}
\boldsymbol{E}(\theta,\phi) &= \sum_n B_n \underbrace{\mathrm{j}\frac{\mathrm{e}^{-\mathrm{j}kr}}{\lambda r}\cos\theta \iint \boldsymbol{f}_n(x,y)\mathrm{e}^{\mathrm{j}(k_x x+k_y y)}\mathrm{d}x\mathrm{d}y}_{\boldsymbol{e}_n(\theta,\phi)}\\
&= \boldsymbol{b}^{\mathrm{T}}\cdot\boldsymbol{e},
\end{aligned} \tag{10}$$

where $\boldsymbol{b}^{\mathrm{T}} = \mathrm{vec}(\boldsymbol{B}) = [B_1,\ldots,B_n]$ is a row vector vectorized from the plane E-field sampling matrix $\boldsymbol{B}$, $\{\cdot\}^{\mathrm{T}}$ represents a transpose, and $\boldsymbol{e} = [\boldsymbol{e}_1(\theta,\phi),\ldots,\boldsymbol{e}_n(\theta,\phi)]$ is a column vector of radiation patterns of orthogonal bases. It is worth noting that the plane orthogonal basis and its far-field radiation pattern are only related to the size of the selected array near-field sampling plane and the division of sampling points. Therefore, for existing MIMO arrays, we only need to estimate the radiation pattern of $\boldsymbol{f}_n(x,y)$

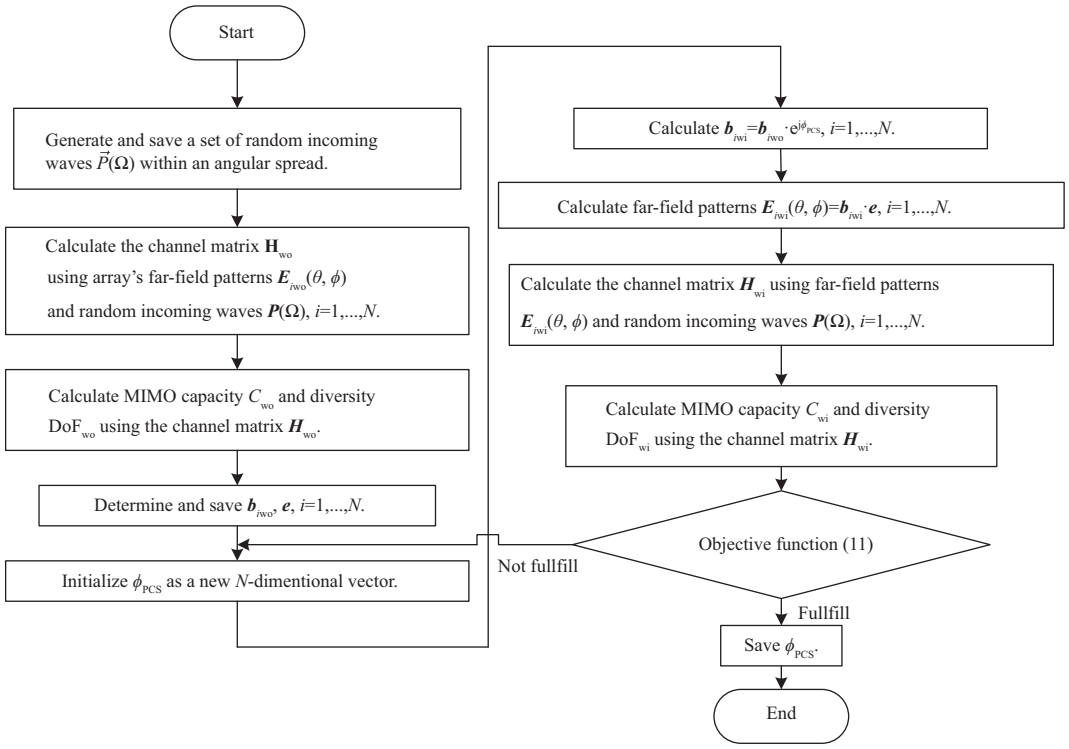

Figure 4 Flow chart of the decorrelation optimization process for an N-ports MIMO array.

once before the optimization process, which can save a lot of time and resources. However, if the array radiation pattern is recalculated every time the PCS phase shift changes during the optimization process, $N_{\mathrm{port}} \times N_{\mathrm{iter}}$ near- to far-field transformations are required, where N_{port}, N_{iter} are the number of array ports and iterations in the optimization process, respectively.

3.3 Optimization algorithm

Our work aims to maximize MIMO capacity by reducing array correlation within a given angular spread, using PCS with optimal phase shift distribution. Thus the objective function is shown as

$$\begin{cases} \text{maximize } f(\phi_{\mathrm{PCS}}) = C_{\mathrm{wi}} - C_{\mathrm{wo}}, \\ \text{subject to } \ \mathrm{DoF}_{\mathrm{wi}} - \mathrm{DoF}_{\mathrm{wo}} > \Delta\mathrm{DoF}, \ f(\phi_{\mathrm{PCS}}) > 0, \end{cases} \tag{11}$$

where subscripts of wi, wo means array with and without PCS, respectively. ΔDoF denotes the improvement that DoF needs to achieve. For a MIMO array with N ports, a flow chart of the whole optimization process is shown in Figure 4.

The optimization algorithm we used is surrogate optimization [36] integrated into MATLAB's global optimization toolbox, which can efficiently find the global optima of the problem [37].

4 Array with PCS loaded

The effectiveness of the decorrelation optimization technique is demonstrated using two antenna arrays. The first is a dual-polarized 1×4 patch array, and we are mainly interested in improving its MIMO performance as an AP in a single-cell scenario (which will be discussed in Subsection 5.1). Another is a 2×8 $\pm 45°$-polarized dipole array specially designed for base stations. Its MIMO performance in both single-cell and multi-cell (will be discussed in Subsection 5.2) will be evaluated.

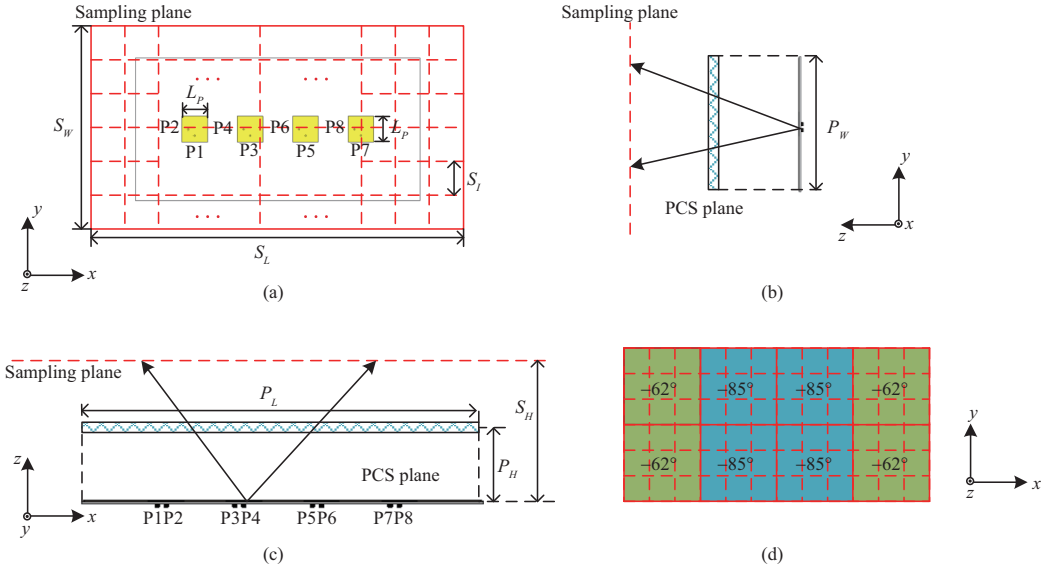

Figure 5 (Color online) Near-field model of patch array. (a)–(c) are front view, side view and top view, respectively. L_p= 28.9, S_W= 800, S_L= 650, S_I= 25, S_H= 150, P_W= 160, P_L= 321, P_H= 87.5 (unit: mm). (d) Optimal phase distribution of the PCS.

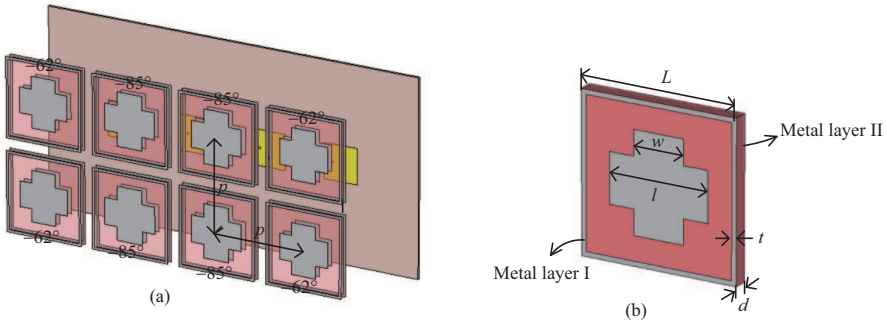

Figure 6 (Color online) (a) Patch array with PCS. (b) PCS element with p = 75, L = 65, d = 6, t = 2, w = 0.5l, l = 42.2 for −62° and 43.3 for −85° (unit: mm).

4.1 Example 1: patch array

We firstly demonstrate the PCS-based near-field optimization technique on a 1 × 4 dual-polarized patch array, as shown in Figure 5. This patch array operates at 2.4 GHz and has an inter-element spacing of 0.5λ (where λ is the free-space wavelength at the design frequency). The dielectric of the patch array is made of a substrate with a relative permittivity of 4.3, a loss tangent of 0.0025, and a thickness of 2 mm. The whole patch array has a size of 321 mm × 160 mm. The near-field channel and its detailed parameters are shown in Figures 5(a)–(c). Near-field sampling plane, PCS is placed at 1.2λ and 0.7λ above the array, respectively. The size of the PCS element is 0.6λ × 0.6λ (75 mm × 75 mm), covering the minimum sampling area of 3 × 3. Therefore in the near-field model, each 3 × 3 sampling area has the same phase shift. For convenience, we mainly focus on the y-polarization of the array. The optimal results of the PCS's phase distribution are shown in Figure 5(d). Moreover, we have checked that this phase distribution can also improve the MIMO performance of the x-polarization of the array.

The PCS element consists of two metal layers with a dielectric layer in the middle, as depicted in Figure 6(b). The top and bottom layers are composed of a square metal ring and a metal cross. The dielectric has a relative permittivity of 2.2, a loss tangent of 0.007, and a thickness of 6 mm. This structure is chosen because it allows a wide transmission phase range and enjoys a simple structure. The patch array with the PCS designed according to Figure 5(d) is shown in Figure 6. It is worth noting that PCS elements should keep the transmission magnitude coefficient above 0.8 (which is needed to avoid degrading the matching and radiation performances of the array).

The proposed PCS in this work is drastically different from the scatterer array presented in [24].

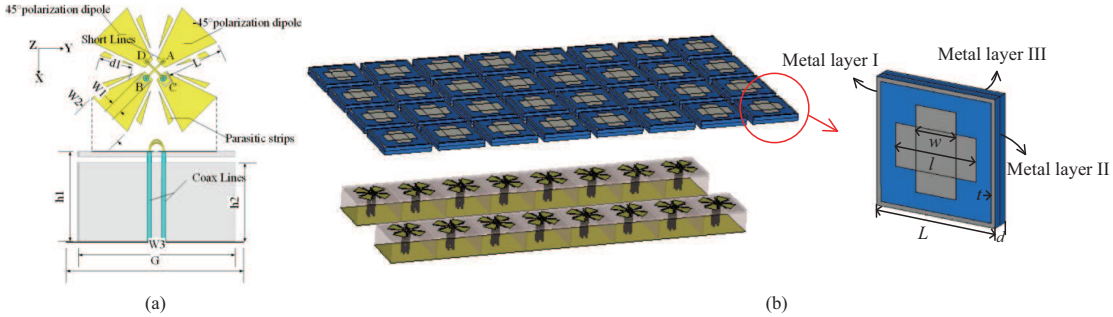

Figure 7 (Color online) BS dipole array with the PCS. (a) Dual-polarized dipole element; (b) configuration of the array together with the PCS. PCS element with $L = 58.33$, $d = 8.75$, $t = 2$, $w = 0.5l$ (unit: mm). l depends on the desired phase shift.

• The scatterer array is essentially a metasurface with periodic (identical) unit cells with a unique transmission coefficient for all the elements. In contrast, the PCS consists of different elements with different transmission phase coefficients at different locations.

• The scatterer array tends to increase the equivalent distances between the array elements by stretching the array elements' phase centers. In contrast, the PCS is obtained by optimizing the phase distribution of the near-field channel.

• Within the horizontal plane for azimuth cellular coverage, the scatterer array becomes less effective for linear arrays with more than four elements. However, the PCS can be applied to an arbitrarily large array (as will be shown in Section 5).

4.2 Example 2: dipole array

To further verify the effectiveness of the PCS-based near-field optimization technique, the BS dual-polarized dipole antenna [38] (cf. Figure 7(a)) in a 2×8 array configuration is used, as shown in Figure 7(b). The array and the PCS are designed to operate at 1.8 GHz. The center-to-center distances between two nearby dipole antennas are 0.38λ in the horizontal direction and 0.7λ in the vertical direction. Since the horizontal angular spread is larger than the vertical angular spread in the typical multipath environment, the horizontal coherence distance is usually smaller than the vertical coherence distance [1, 39]. Therefore, the antenna spacing in the horizontal direction is usually smaller than that in the vertical direction in practice [40, 41]. For this example, the PCS element has the same crossed shape used in Example 1. In this example, we choose PCS elements with smaller sizes as they can change phase distribution over array aperture elaborately. Though PCS elements with smaller sizes usually have a narrow phase range, their phase range can still become wider using more layers [42]. It consists of three metal layers with two dielectric layers in the middle, as shown in Figure 7(b). The spacing between the center points of adjacent PCS elements is 0.4λ, and the dielectric has a relative permittivity of 4. The interval of the near-field sampling plane is $S_I = 0.2\lambda$. The parameters of the near-field model and the optimal result of the PCS phase distribution are shown in Figure 8. The whole optimization process with 800 iterations takes about 13 min on a personal computer when the near-field sampling matrix $\boldsymbol{B}_{\text{wo}}$ and the orthogonal basis's far-field pattern vector $\boldsymbol{e}$ have already been created and saved in the computer. It should be mentioned that during optimization, we only focus on optimizing $+45°$ polarization due to the symmetry of the array.

In Section 5, we will evaluate the MIMO performances of the two examples in multipath environments.

5 MIMO performance evaluations

In order to demonstrate the effectiveness of the proposed decorrelation optimization techniques, we evaluate the two arrays in Section 4 with and without the PCSs in different multipath scenarios.

5.1 Performance evaluation in single-cell scenario

To evaluate the MIMO performances of the two examples, we first resort to a ray-tracing-based in-house channel emulator that has been used in [16]. We assume the arrays under evaluation cover one sector of 120° at an AP/BS site with a reference SNR of 15 dB, and the number of users (each equipped

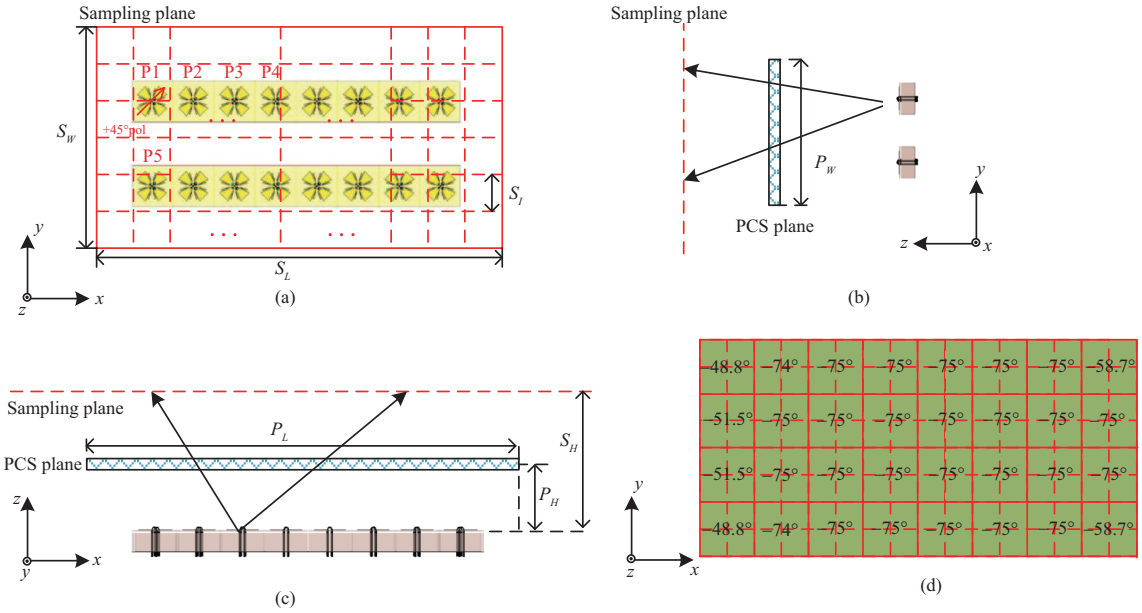

Figure 8 (Color online) Near-field model of diople array. (a)–(c) are front view, side view and top view, respectively. S_W = 1166, S_L = 1433, S_I = 33.3, S_H = 200, P_W = 303, P_L = 586, P_H = 133 (unit: mm). (d) Optimal phase distribution of the PCS.

with a single-polarized antenna) is equal to the number of AP/BS antenna ports. For simplicity, we further assume a single-cell scenario in the uplink mode, where the uncorrelated user equipment (UEs) are uniformly distributed along an arc with an origin that coincides with the AP/BS site. Thus, the simulation scenarios are equivalent to an 8×8 MIMO system for the patch array (i.e., Subsection 4.1) and a 32×32 MIMO system for the dipole array (i.e., Subsection 4.2), both with uncorrelated transmitting antennas. The simplified simulation setup allows a closer examination of the channel angular spread effect on the MIMO performance. A more sophisticated channel model will be employed for the multi-cell scenario in Subsection 5.2.

We import the (complex-valued) embedded radiation patterns of the AP/BS arrays into the channel emulator. The channel coefficients are emulated by impinging incident waves on the radiation patterns [16, 21]. Specifically, for each run of the channel emulation, 100 subpaths are generated for each UE. We assume these subpath channels of all the UEs are uniformly distributed within a limited angular spread with the mean incident angle impinging at the broadside of the AP/BS array, as illustrated in Figure 9(a). Note that other angular distributions can be used as well. Nevertheless, it is well known that the spatial correlation is mainly determined by the angular spread instead of the shape of the angular distribution [43]. To account for the random orientations of the UE, we assume the linearly polarized incident waves have a unity cross-polarization ratio. This procedure is repeated 10000 times for each UE and each angular spread. In total, we simulated ten angular spread cases ranging from 0° to 90°. Once all the channel snapshots are gathered, the 10000 channel realizations are used to calculate the diversity measure (i.e., correlation performance) and the ergodic capacity.

The simulated MIMO performances of the patch arrays (i.e., Subsection 4.1) are shown in Figure 10. As can be seen, the PCS improves the diversity measure (i.e., overall correlation performance) by about 7% and the capacity by about 8%, averaged over different angular spreads.

Figure 11(a) shows the MIMO performances of the dipole array (i.e., Subsection 4.2). As can be seen, with the PCS, the diversity measure is improved by about 9% and the capacity by about 8% averaged over different angular spreads. From both examples, it is safe to conclude that the PCS-based near-field optimization technique can effectively improve the MIMO performances of the two arrays.

It is noted that the antenna characteristics (such as mismatches and efficiencies) are included in the embedded radiation patterns and also included in the MIMO performances. We focus on the MIMO performances in this subsection, while the antenna S-parameters and radiation patterns are deferred till Section 6. It is worth pointing out that the ultimate goal of the PCS-based near-field optimization technique is to increase the MIMO capacity (by increasing the diversity measure of the channel) instead of improving the conventional antenna characteristics. Next, a simulation for the MIMO performance

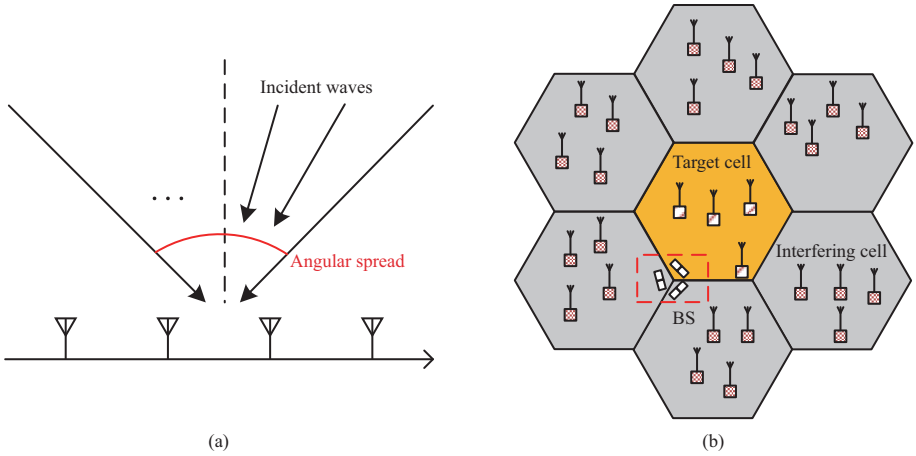

Figure 9 (Color online) (a) Angular distribution of incident waves; (b) illustration of the multi-cell scenario.

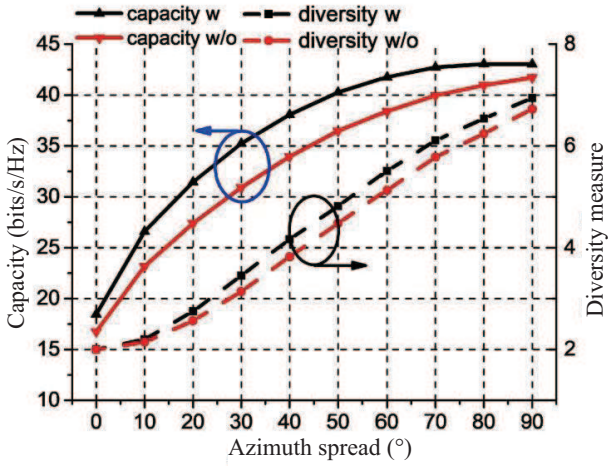

Figure 10 (Color online) Simulated patch MIMO array performance: diversity measures (dashed lines) and capacities (solid lines) of the patch array with (black) and without (red) the PCS.

of the dipole array working as a BS in a multi-cell scenario is conducted to further verify the proposed decorrelation technique.

5.2 Performance evaluation in multi-cell scenario

Figure 9(b) shows an illustration of the multi-cell simulation setup. The BS array under evaluation serves the target cell in the middle. To account for inter-cell interferences, we add six interfering cells surrounding the target cell (i.e., a one-tier layout). Within each cell, there are four UEs, each equipped with a vertical half-wavelength dipole antenna. Since the BS antennas are dual-polarized with 45° [40,41], the actual orientation of the UE antenna is less important in the statistical sense. The cell has a radius of 166.7 m. The UEs are 1.5 m above the ground, while the base station has a height of 25 m with a 7° down tilt, as a typical BS setup. For link channel emulations, we resort to the geometry-based stochastic WINNER+ channel model [44]. Specifically, the urban micro (Umi) channel model in the non-line-of-sight scenario is selected. Thus, for each subchannel (between a UE and the BS array), there are 16 clusters. Each cluster is composed of 20 subpaths. It has been proved in [45] that such cluster-based model structures can obtain satisfactory accuracy of modeling while significantly reducing complexity. In each drop (realization), the UEs are assigned random locations, and all the subchannels (with both useful channels and intra/inter-cell interference channels) are simulated and gathered. Due to the interference channels' presence, in the calculation of the sum capacity (i.e., the total capacity of all the UEs in the target cell), the reference SNR γ in (1) should be replaced with the signal-to-interference-plus-noise ratio (SINR). Since the clusters (each with a random angular spread whose statistics are predefined in the Umi channel model) are randomly generated in each drop, one cannot control the channel's angular spread

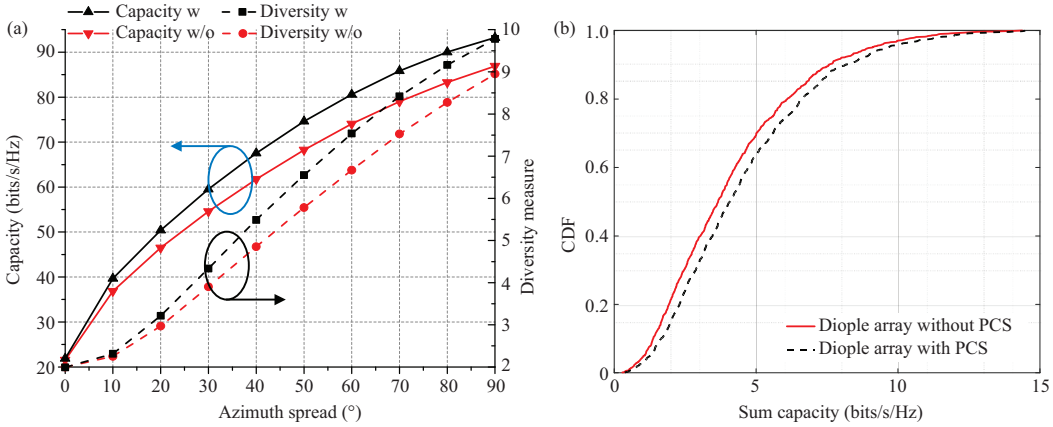

Figure 11 (Color online) (a) Simulated dipole MIMO array performance: diversity measures (dashed lines) and capacities (solid lines) of the BS dipole array with (black) and without (red) the PCS. (b) CDF of the sum capacity of the BS dipole array with and without the PCS in the multi-cell Umi channel scenario.

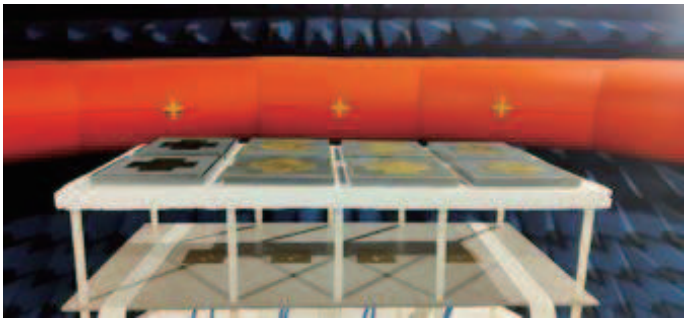

Figure 12 (Color online) Prototype photo of the patch array with the PCS.

as in the previous subsection. Moreover, since the UE locations are randomly assigned within their corresponding cells in each drop, different UEs will experience different path losses. In this case, it is more suitable to present the MIMO performance in terms of the cumulative distribution function (CDF) of the instantaneous capacity instead of the ergodic capacity as in Subsection 5.1. In total, 1000 drops are generated to obtain the CDF of the sum capacity.

Figure 11(b) shows the CDF of the sum capacity of the BS dipole array in the multi-cell scenario. As can be seen, the PCS improves the sum capacity by about 10% on average. Note that the ray-tracing emulator used in Subsection 5.1 produces normalized channel coefficients (i.e., does not include the actual pass loss) with 32 UEs for the BS dipole array in the single-cell scenario (without inter-cell interference). In contrast, the WINNER+ channel model used in this subsection includes the path losses of the UEs as well as intra- and inter-cell interferences. Therefore, the sum capacity in the multi-cell scenario is lower than that in the single-cell scenario. Nevertheless, the primary purpose of this study is to show the MIMO performance improvement by the proposed PCS-based near-field optimization technique. From all the simulation results, it is safe to conclude that the proposed technique can effectively improve the MIMO performance of a BS array.

6 Array antenna characteristics

For the fabrication and measurement convenience, only the patch array with the corresponding PCS is manufactured and measured to show the PCS effects on the conventional antenna characteristics. Figure 12 shows the prototype of the patch array together with the PCS in a multi-probe anechoic chamber. A foam (with a relative permittivity close to unity) with ten thin Nylon columns supports the discretized PCS. Full-wave simulations in CST have verified that the supporting structure has a negligible effect on the antenna characteristics.

Figure 13 shows the simulated and measured S-parameters of the patch array with (w) the PCS. The S-parameters without (w/o) the PCS are plotted in the same figures for comparison. Due to the

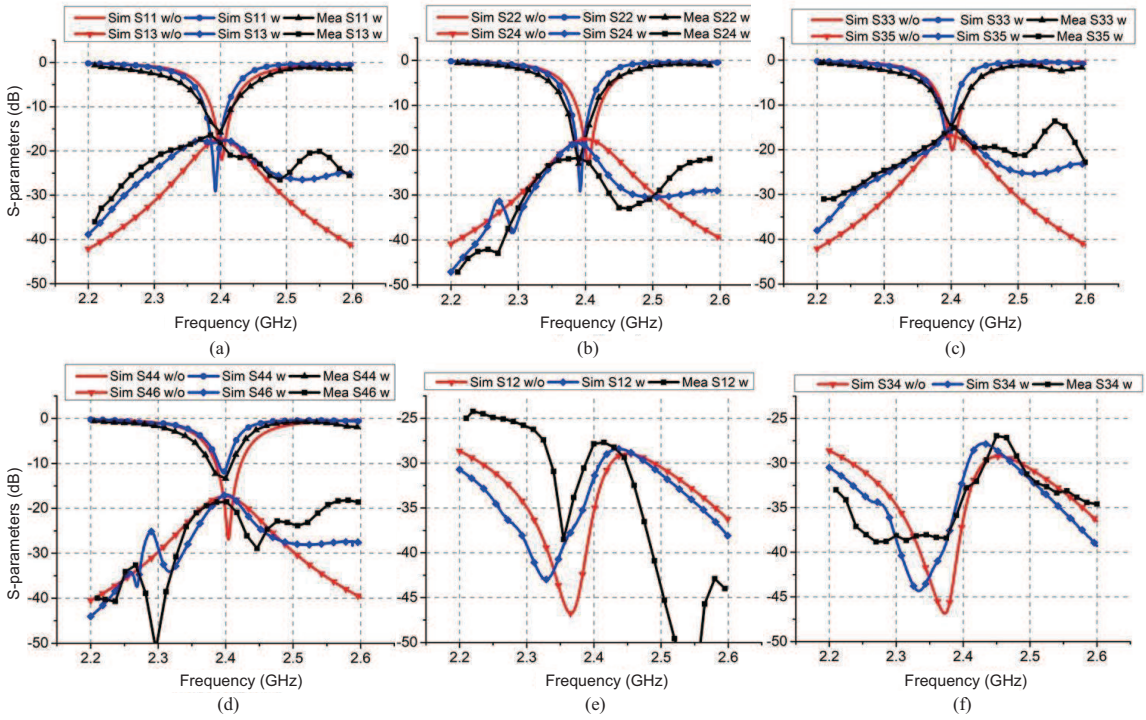

Figure 13 (Color online) Simulated and measured S-parameters: (a) S11, S13, (b) S22, S24, (c) S33, S35, (d) S44, S64, (e) S12, and (f) S34. The port indices are marked in Figure 5.

array's symmetry, only parts of the S-parameters are shown here. As can be seen, there are good agreements between the measured and simulated S-parameters of the patch array with the PCS, except for the polarization coupling of the left-most patch element S12 (where a noticeable difference is observed). Nevertheless, since the measured and simulated S12 are below −25 dB already, the difference is insignificant. Moreover, it can be seen that the PCS has only insignificant effects on the mutual couplings of the patch array. The same condition is also shown in the dipole array, whose simulated S-parameters between adjacent antenna elements are shown in Table 1, in which the port number index refers to ports of +45°-polarization shown in Figure 8.

Since the goal of the PCS is to change the phase distribution in the near-field of the array to achieve better MIMO performances, the PCS will inevitably alter the radiation patterns of the array elements, as shown in Figure 14. Due to the symmetry of the array configuration, only co- and cross-polarization radiation patterns of two elements on the left of the array (i.e., Ports 1–4 marked in Figure 5) with and without the PCS are plotted in Figure 14. In general, good agreements are observed between the simulated and measured radiation patterns of the patch array elements in the presence of the PCS. The simulated radiation patterns of the array elements without the PCS are also plotted in the same figures to show the PCS effect on the radiation patterns. As expected, there are apparent changes in the radiation patterns after loading the array with the PCS. The beamwidths in the yz-plane (corresponding to the vertical plane in the MIMO channel simulations) are reduced. This effect tends to reduce the overlapping of the radiation patterns and slightly increase the gain of antennas. Moreover, since the elevation angular spread in the multipath channel is usually much smaller than that of the azimuth elevation angular spread [44], the reduced elevation beamwidth does not reduce the received power and often tends to increase the received power and suppress the inter-cell interferences. In fact, this is also the reason that real-life BSs usually employ subarrays in the vertical direction [46, 47]. With the PCS's help, fewer elements are required to construct the vertical subarray, which is a merit of the PCS. Moreover, these apparent changes in the antenna array's radiation patterns make the corresponding intra-cell subchannels orthogonal to each other. Finally, decorrelate array antennas and improve the MIMO capacity of the array.

Since the horizontal arrays are usually operated as MIMO antennas, it is vital to make the radiation patterns in the horizontal plane orthogonal to each other [21]. The objective function shown in (11) can effectively decorrelate an existing MIMO array and ensure the improvement in MIMO capacity.

Table 1 Mutual couplings of the dipole array in Example 2[a)]

	S12	S23	S34	S15
Without PCS	−16.6	−18.7	−16.6	−31.7
With PCS	−16.2	−17.9	−16.5	−32

a) All S-parameters are in dB and simulated at 1.8 GHz. For each port, such as the port i, Sii is below −10 dB.

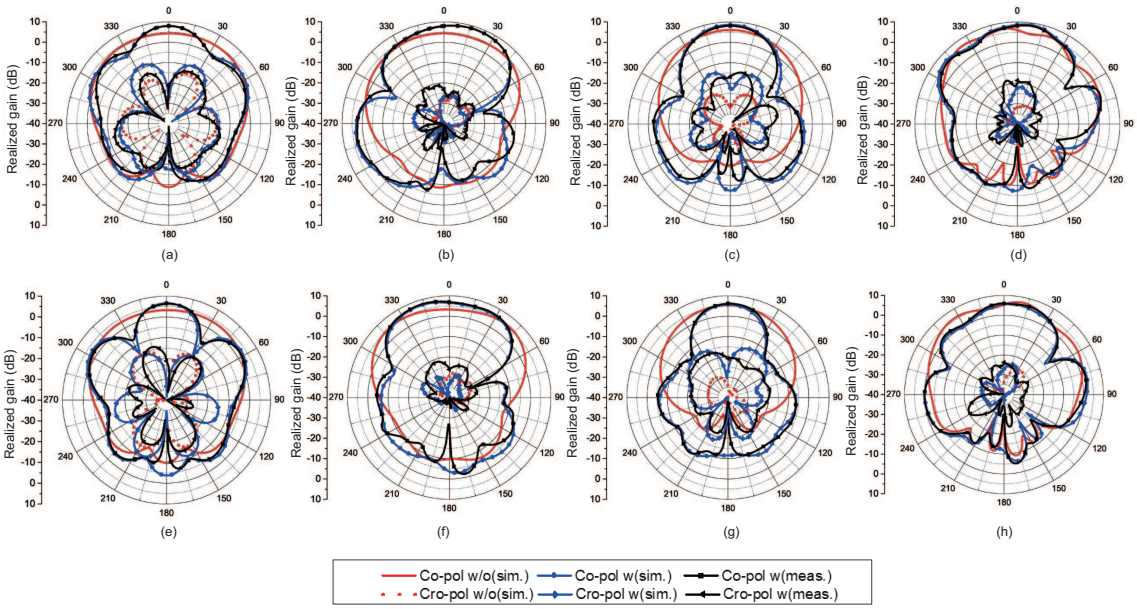

Figure 14 (Color online) Simulated and measured radiation patterns of the patch array with and without the PCS at 2.4 GHz. (a) and (b) correspond to Ports 1, (c) and (d) correspond to Ports 2, (e) and (f) correspond to Ports 3, (g) and (h) correspond to Ports 4, (a), (c), (e), (g) correspond to yz-plane, and (b), (d), (f), (h) correspond to xz-plane. The coordinates are shown in Figure 5.

Therefore, we have achieved a similar optimization goal of [21] by using the proposed PCS. As opposed to the theoretical work in [21], which does not consider the implementation of practical MIMO antennas, this work presents a simple yet effective procedure to enhance the MIMO performances. Furthermore, the effectiveness of the proposed PCS has been validated using various MIMO channel simulations for both single-cell and multi-cell scenarios.

This work assumes that the BS or AP arrays are installed with a priori knowledge about the locations of all potential users so that the mean incident angle is close to the broadside of the array. In future work, it might be helpful to make the PCS reconfigurable [48, 49] to match the instantaneous angular distribution of the incident waves, which is not difficult to achieve with the decorrelation optimization technique based on the near-field channel model. This can be especially rewarding for the beyond 5G millimeter-wave BS scenarios, where the channel subpaths become irregular and sparse. Moreover, it is firstly revealed that channel sparsity can be observed at the sub-6GHz band and it has high instability, and solid evidence is provided in [39]. Nevertheless, for the considered sub-6 GHz communication, the proposed PCS-based near-field optimization technique provides an effective yet inexpensive solution to MIMO performance enhancement in a statistical sense.

To further illustrate the new contributions of this work, relevant studies are summarized in the comparison table below. Note that all the studies listed in Table 2 can effectively enhance the MIMO performances in different multipath scenarios. As mentioned before, the correlations and MIMO capacities depend on the MIMO arrays as well as the propagation environments (e.g., the channel angular spreads). Therefore, it would be unfair to directly compare the actual capacity improvements of the listed studies since their array configurations and assumed multipath environments are different. For instance, it is well known that a small angular spread can yield severe correlation degradation for a MIMO array with half-wavelength (or even larger) inter-element separation, whereas the correlations between half-wavelength separated antennas are close to zero in an isotropic scattering environment [1]. Unlike the beam tilting schemes [19, 20, 23, 26] (which are more suitable for MIMO terminals), Refs. [24, 25], and this work can achieve decorrelation while keeping broadside radiations, which is vital for providing good

Table 2 Comparison with previous studies[a)]

Ref.	Array config.	Decorrelation method	Multipath scenario
[17]	1×4	–	Isotropic/indoor (single cell)
[19]	1×2	Beam tilting	Isotropic (single cell)
[20]	2×3	Beam tilting	Isotropic (single cell)
[26]	4-port (irregular)	Beam tilting	Isotropic (single cell)
[23]	1×2	Beam tilting	Isotropic (single cell)
[24]	1×4	Stretching phase center distance	Non-isotropic (single cell)
[25]	1×4	Stretching phase center distance	Non-isotropic (single cell)
This work	2×8	Near-field optimization technique	Non-isotropic (single- & multi-cell)

a) Among the listed schemes, only the proposed near-field optimization technique can be applied to large MIMO arrays.

cellular coverage for BS/AP applications. As opposed to the previous studies (including [24,25]) that are mainly limited to small arrays, the proposed PCS can be extended to large BS arrays. Unlike the previous studies [17–26] that have only been validated in single-cell scenarios, the effectiveness of the proposed PCS-based near-field optimization technique has been demonstrated with realistic multipath channel models in both single- and multi-cell scenarios. Though the PCS-based near-field optimization technique requires more design complexity in the algorithm design process and design of elements with different transmission coefficients, it is effective for massive MIMO arrays and complex multipath scenarios.

7 Conclusion

This paper proposes the PCS-based near-field optimization technique for MIMO performance enhancement, which has provided a new perspective for better MIMO array designs. In non-isotropic multipath scenarios, the effects of correlations between the array antenna elements on MIMO performance have been discussed. A near-field channel model and an optimization process have been introduced to obtain a better near-field phase distribution over the array's aperture. Then, the PCS has been designed to achieve target near-field phase distribution. Two arrays with different antenna types and array sizes were used to demonstrate the proposed technique's effectiveness. For a 1×4 dual-polarized patch array, MIMO performances can be effectively enhanced by 8% in single-cell scenarios. Moreover, the PCS-based near-field optimization technique could improve the MIMO performance by 8% and 10% for the 2×8 BS dipole array in single-cell, and multi-cell scenarios, respectively. Furthermore, array antenna characteristics of the 1×4 dual-polarized patch array have been discussed, showing that PCS has insignificant effects on matching and isolation performances of the array, and changes in radiation patterns benefit the diversity and MIMO capacity of the array. Unlike the previous decorrelation studies that are mainly confined to small MIMO arrays, the PCS-based near-field optimization technique can be applied to large BS arrays, effectively improving MIMO performance for it can reduce the correlations in a large MIMO array while keeping broadside radiations to ensure good cellular coverage.

Acknowledgements This work was supported in part by National Natural Science Foundation of China (Grant No. 62171362).

References

1 Paulraj A, Rohit A P, Nabar R, et al. Introduction to Space-Time Wireless Communications. Cambridge: Cambridge University Press, 2003
2 Zaidi A, Athley F, Medbo J, et al. 5G Physical Layer: Principles, Models and Technology Components. Pittsburgh: Academic Press, 2018
3 Wang D M, Zhang Y, Wei H, et al. An overview of transmission theory and techniques of large-scale antenna systems for 5G wireless communications. Sci China Inf Sci, 2016, 59: 081301
4 Mikki S M, Antar Y M M. On cross correlation in antenna arrays with applications to spatial diversity and MIMO systems. IEEE Trans Antennas Propagat, 2015, 63: 1798–1810
5 Wang Z, Zhao L, Cai Y, et al. A meta-surface antenna array decoupling (MAAD) method for mutual coupling reduction in a MIMO antenna system. Sci Rep, 2018, 8: 3152
6 Tang J, Faraz F, Chen X, et al. A metasurface superstrate for mutual coupling reduction of large antenna arrays. IEEE Access, 2020, 8: 126859–126867
7 Sarkar D, Saurav K, Srivastava K V. Dual band complementary split-ring resonator-loaded printed dipole antenna arrays for pattern diversity multiple-input-multiple-output applications. IET Microwaves Antenna Propagation, 2016, 10: 1113–1123
8 Gao Y, Ma R, Wang Y, et al. Stacked patch antenna with dual-polarization and low mutual coupling for massive MIMO. IEEE Trans Antennas Propagat, 2016, 64: 4544–4549
9 Wang X, Feng Z H, Luk K-M. Pattern and polarization diversity antenna with high isolation for portable wireless devices. Antenna Wirel Propag Lett, 2008, 8: 209–211
10 Chiu C Y, Cheng C H, Murch R D, et al. Reduction of mutual coupling between closely-packed antenna elements. IEEE Trans Antenna Propagat, 2007, 55: 1732–1738
11 Wang H, Liu L, Zhang Z, et al. A wideband compact WLAN/WiMAX MIMO antenna based on dipole with V-shaped ground branch. IEEE Trans Antennas Propagat, 2015, 63: 2290–2295

12 Diallo A, Luxey C, Le Thuc P, et al. Study and reduction of the mutual coupling between two mobile phone PIFAs operating in the DCS1800 and UMTS bands. IEEE Trans Antenna Propagat, 2006, 54: 3063–3074
13 Rajo-Iglesias E, Quevedo-Teruel Ó, Inclan-Sanchez L. Mutual coupling reduction in patch antenna arrays by using a planar EBG structure and a multilayer dielectric substrate. IEEE Trans Antenna Propagat, 2008, 56: 1648–1655
14 Tan X, Wang W, Wu Y, et al. Enhancing isolation in dual-band meander-line multiple antenna by employing split EBG structure. IEEE Trans Antenna Propagat, 2019, 67: 2769–2774
15 Sun L, Li Y, Zhang Z, et al. Antenna decoupling by common and differential modes cancellation. IEEE Trans Antenna Propagat, 2020, 69: 672–682
16 Chen X, Pei H, Li M, et al. Revisit to mutual coupling effects on multi-antenna systems. J Commun Inf Netw, 2020, 5: 411–422
17 Zhang Y, Shen S, Han Z, et al. Compact MIMO systems utilizing a pixelated surface: capacity maximization. IEEE Trans Veh Technol, 2021, 70: 8453–8467
18 Pedersen G F, Andersen J B. Handset antennas for mobile communications: integration, diversity and performance. Rev Radio Sci, 1999, 5: 119–137
19 Hassan T, Khan M U, Attia H, et al. An FSS based correlation reduction technique for MIMO antennas. IEEE Trans Antenna Propagat, 2018, 66: 4900–4905
20 Das G, Sharma A, Gangwar R K, et al. Performance improvement of multiband MIMO dielectric resonator antenna system with a partially reflecting surface. Antenna Wirel Propag Lett, 2019, 18: 2105–2109
21 Quist B T, Jensen M A. Optimal antenna radiation characteristics for diversity and MIMO systems. IEEE Trans Antenna Propagat, 2009, 57: 3474–3481
22 Sarkar D, Mikki S, Antar Y M M. Engineering the eigenspace structure of massive MIMO links through frequency-selective surfaces. Antennas Wirel Propag Lett, 2019, 18: 2701–2705
23 Qureshi U, Khan M U, Sharawi M S, et al. Field decorrelation and isolation improvement in an MIMO antenna using an all-dielectric device based on transformation electromagnetics. Sensors, 2021, 21: 7577
24 Wang Y, Chen X, Liu X, et al. Improvement of diversity and capacity of MIMO system using scatterer array. IEEE Trans Antenna Propagat, 2021, 70: 789–794
25 Li M, Chen X, Zhang A, et al. Reducing correlation in compact arrays by adjusting near-field phase distribution for MIMO applications. IEEE Trans Veh Technol, 2021, 70: 7885–7896
26 Das G, Sahu N K, Sharma A, et al. FSS-based spatially decoupled back-to-back four-port MIMO DRA with multidirectional pattern diversity. Antennas Wirel Propag Lett, 2019, 18: 1552–1556
27 Chen X, Zhao M, Huang H, et al. Simultaneous decoupling and decorrelation scheme of MIMO arrays. IEEE Trans Veh Technol, 2021, 71: 2164–2169
28 Guan K, Li G, Kurner T, et al. On millimeter wave and THz mobile radio channel for smart rail mobility. IEEE Trans Veh Technol, 2016, 66: 5658–5674
29 Ivrlac M T, Nossek J A. Diversity and correlation in Rayleigh fading MIMO channels. In: Proceedings of IEEE 61st Vehicular Technology Conference, 2005. 151–155
30 Bretherton C S, Widmann M, Dymnikov V P, et al. The effective number of spatial degrees of freedom of a time-varying field. J Clim, 1999, 12: 1990–2009
31 Xu Z, Liu Y, Li M, et al. Linearly polarized shaped power pattern synthesis with dynamic range ratio control for arbitrary antenna arrays. IEEE Access, 2019, 7: 53621–53628
32 Zhang H, Shlezinger N, Guidi F, et al. Beam focusing for near-field multiuser MIMO communications. IEEE Trans Wireless Commun, 2022, 21: 7476–7490
33 Xu J, You L, Alexandropoulos G C, et al. Near-field wideband extremely large-scale MIMO transmission with holographic metasurface antennas. 2022. ArXiv:220502533
34 Senior T B, Volakis J L. Approximate Boundary Conditions in Electromagnetics. London: The Institution of Engineering and Technology, 1995
35 Gregson S, McCormick J, Parini C. Principles of Planar Near-Field Antenna Measurements. London: The Institution of Engineering and Technology, 2007
36 Gutmann H M. A radial basis function method for global optimization. J Glob Optimization, 2001, 19: 201–227
37 Koziel S. Simulation-Driven Design Optimization and Modeling for Microwave Engineering. Singapore: World Scientific, 2013
38 Li M, Chen X, Zhang A, et al. Dual-polarized broadband base station antenna backed with dielectric cavity for 5G communications. IEEE Antennas Wireless Propag Lett, 2019, 18: 2051–2055
39 He R, Ai B, Wang G, et al. Wireless channel sparsity: measurement, analysis, and exploitation in estimation. IEEE Wireless Commun, 2021, 28: 113–119
40 He R, Ai B, Stuber G L, et al. Geometrical-based modeling for millimeter-wave MIMO mobile-to-mobile channels. IEEE Trans Veh Technol, 2017, 67: 2848–2863
41 Wu K L, Wei C, Mei X, et al. Array-antenna decoupling surface. IEEE Trans Antenna Propagat, 2017, 65: 6728–6738
42 Abdelrahman A H, Yang F, Elsherbeni A Z, et al. Analysis and Design of Transmitarray Antennas. Cham: Springer, 2017. 6: 1–175
43 Andersen J B, Pedersen K I. Angle-of-arrival statistics for low resolution antennas. IEEE Trans Antennas Propagat, 2002, 50: 391–395
44 Meinilä J, Kyösti P, Hentilä L, et al. WINNER+ Final Channel Models, Deliverable D5.3 V1.0, 30 Jun. 2010. http://projects.celtic-initiative.org/winner+/index.html
45 He R, Schneider C, Ai B, et al. Propagation channels of 5G millimeter-wave vehicle-to-vehicle communications: recent advances and future challenges. IEEE Veh Technol Mag, 2019, 15: 16–26
46 Wu R, Chu Q X. A compact, dual-polarized multiband array for 2G/3G/4G base stations. IEEE Trans Antenna Propagat, 2019, 67: 2298–2304
47 Ye L H, Zhang X Y, Gao Y, et al. Wideband dual-polarized two-beam antenna array with low sidelobe and grating-lobe levels for base-station applications. IEEE Trans Antenna Propagat, 2019, 67: 5334–5343
48 Farzami F, Khaledian S, Smida B, et al. Pattern-reconfigurable printed dipole antenna using loaded parasitic elements. Antenna Wirel Propag Lett, 2016, 16: 1151–1154
49 Yuan J, Wen M, Li Q, et al. Receive quadrature reflecting modulation for RIS-empowered wireless communications. IEEE Trans Veh Technol, 2021, 70: 5121–5125